$AlCl_3$ coordinating interlayer spacing in microcrystalline graphite facilitates ultra-stable and high-performance sodium storage

Zheng Li,[a] Zhongliang Tian,*[a] Chengzhi Zhang,*[b,d] Fei wang,[c,d] Chong Ye,[c] Fei Han,[c] Jun Tan,*[b] and Jinshui Liu[c]

[a] *School of Metallurgy and Environment, Central South University, Changsha 410082, China*

[b] *Ji Hua Laboratory, Foshan, Guangdong, 528000, China*

[c] *Hunan Province Key Laboratory for Advanced Carbon Materials and Applied Technology, College of Materials Science and Engineering, Hunan University, Changsha, Hunan, 410082, China*

[d] *Shenyang National Laboratory for Materials Science, Institute of Metal Research, Chinese Academy of Sciences, Shenyang, 110016, China*

*Corresponding authors

E-mail: tianzhongliang@csu.edu.cn, zhangchz@jihualab.com, tanjun@jihualab.com

Experimental Section

Preparation of $AlCl_3$-intercalated GICs : The $AlCl_3$-intercalated GICs were directly provied by a molten-salt method. In a typical procedure, the raw materials of microcrystalline graphite (99.5%), $AlCl_3$ were firstly dried in a vacuum oven at 80 °C to remove the surface-adsorbed water. Then, 2.0 g of microcrystalline graphite were quickly mixed with 10 g $AlCl_3$ salts in a mortar, and the mixture was placed into a sealed stainless-steel autoclave (Anhui Kemi Machinery Technology Co., Ltd). Subsequently, the autoclave was continuously heated at 180 °C for 10 h with a heating rate of 5 °C min^{-1}. After cooling, the powder was washed in turn with ethanol, 0.1M of HCl solution and deionized water to remove the residual reactants. After drying at 80 °C, the $AlCl_3$-intercalated GICs were obtained.

Materials characterization : The structure evolution of samples were monitored by X-raydiffraction (XRD, TD-3300) with Cu Kα radiation (λ = 1.5406 Å) at a scanning step of 0.02° and Labram-010 Raman microscope with an excitation wavelength of 514.5 nm. The pore parameters were measured by nitrogen adsorption technique with a Micromeritics Tristar 3000 instrument at 77 K. The morphology and microstructure were studied by field-emission scanning electron microscope (SEM, Sigma HD) and Titan G2 60-300 high-resolution transmission electron microscope (TEM). X-ray photoelectron spectroscope (XPS) analysis was operated using an ESCALAB 250XI system with a monochromatic Al K source.

Electrochemical measurements : The working electrodes were made by mixing polyvinylidene fluoride (10 wt%), conductive carbon black (20 wt%) and the active materials (70 wt%) in water/ ethanol mixture, and coating the electrode slurry mixture on the copper foil. The mass loading of typical active substances on each Cu foil is

about 1.0 ~ 1.5mg cm^{-2}. The ester-based electrolyte was 1 M $NaPF_6$ in EC (ethylene carbonate) and DEC (diethyl carbonate) mixture (1:1, v/v), and the ether-based electrolyte is 1 M $NaPF_6$ in DEGDME (diethylene glycol dimethyl ether), DME (ethylene glycol dimethyl ether) and TEGDME (tetraethylene glycol dimethyl ether). Electrochemical tests were carried out in type 2025 coin cells assembled at an argon atmosphere in a glove box. The half-cells test voltage range of the coin type was 0.005 - 3 V, tested on the land-based CT2001A battery tester. The electrochemical impedance was measured from 100 kHz to 0.1 Hz at the Gamry interface 1000E electrochemical workstation. The cyclic voltammetry (CV) curve was recorded at CHI660E electrochemical workstation, and the scanning rate was 0.2 mV s^{-1}.

DFT Computational Methods : Geometric optimizations of $[Na\text{-}DME]^+$, $[Na\text{-}DEGDME]^+$ and $[Na\text{-}TEGDME]^+$ complexes were performed with the DFT platform using DMol[3] package[1] and Gaussian program[2]. All the structures were optimized at the B3LYP level.

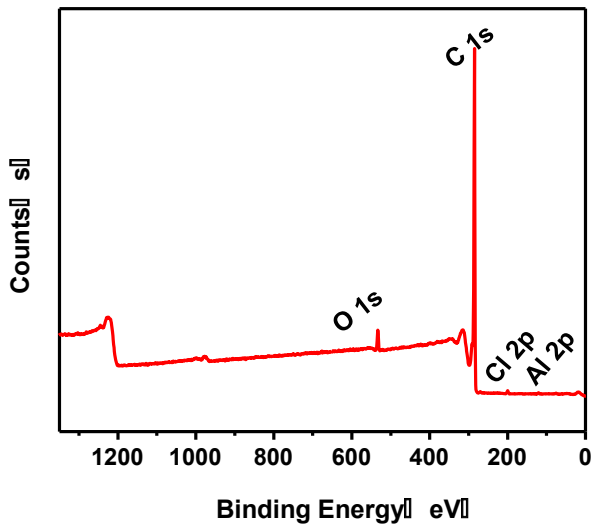

Fig. S1 XPS profiles of $AlCl_3$-MGIC.

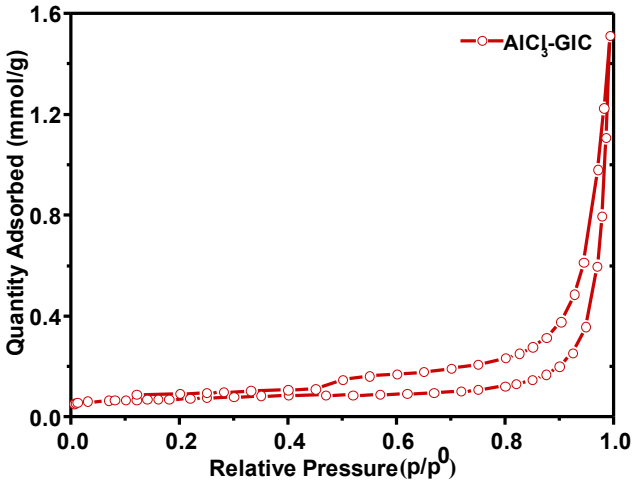

Fig. S2 N_2 sorption isotherm of the $AlCl_3$-MGIC sample.

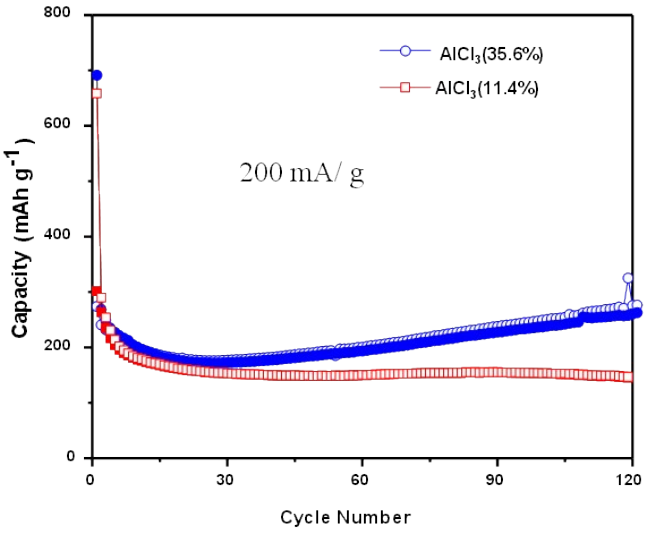

Fig. S3 Cycling performance of different $AlCl_3$ content samples at a current density of 0.2 A g^{-1}.

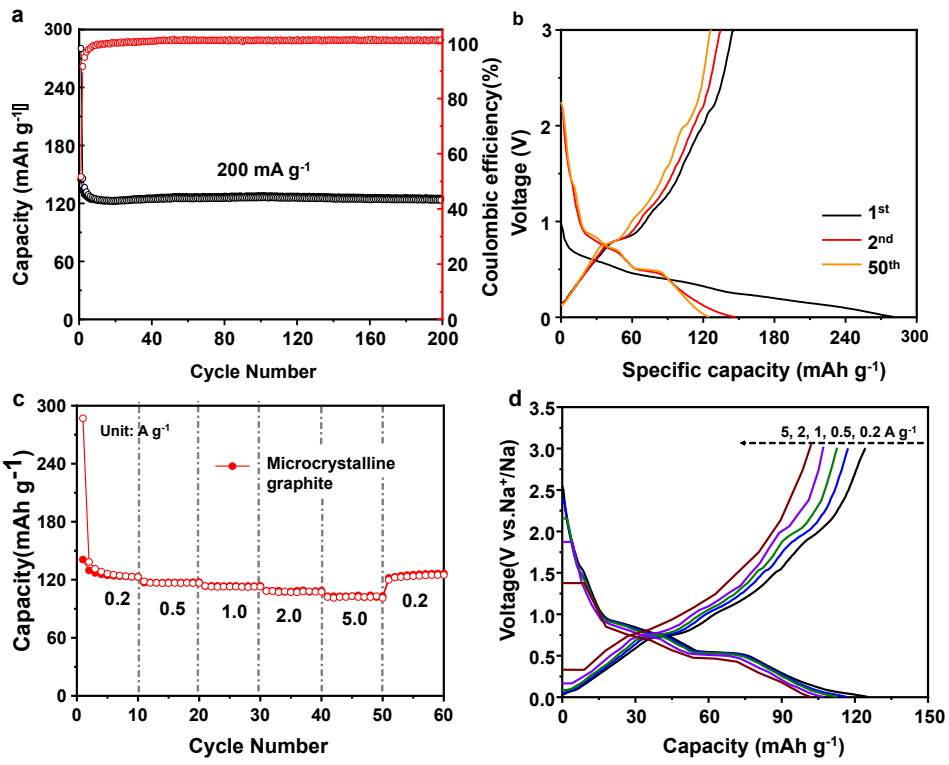

Fig. S4 (a) cycle performance, (b) galvanostatic discharge/charge profiles, (c) rate performance, and (d) discharge/charge profiles of MG in DEGDME electrolyte.

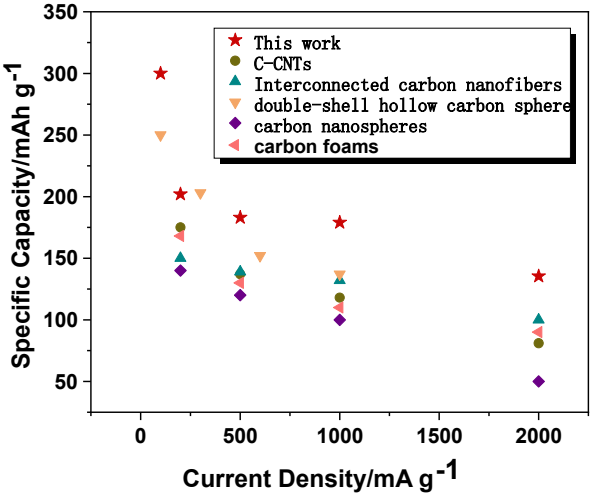

Fig. S5 Rate comparison of the current work and other carbon-based anode materials for SIBs.

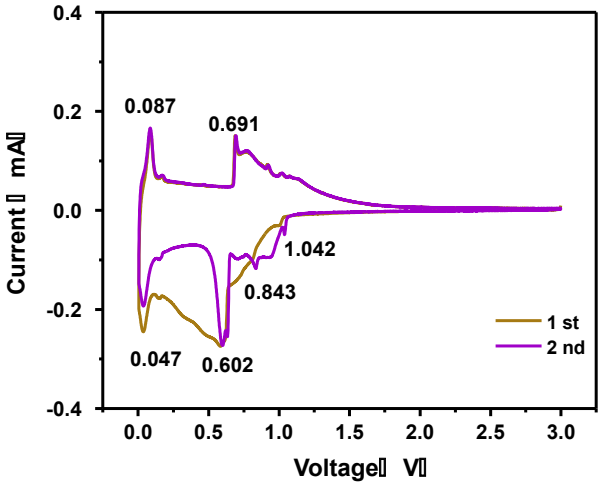

Fig. S6 Cyclic voltammograms of the graphite anode at 0.2 mV s^{-1} for SIBs.

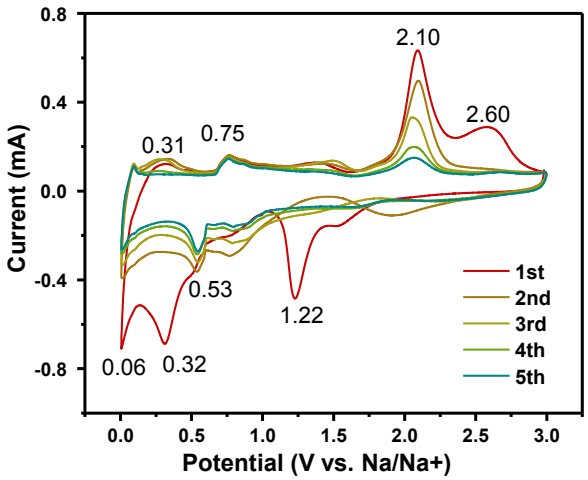

Fig. S7 Cyclic voltammograms of the DEGDME anode at 0.2 mV s^{-1} for SIBs.

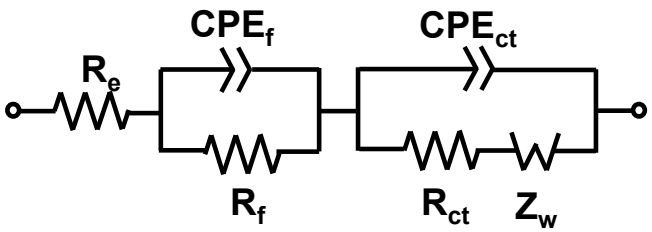

Fig. S8 Equivalent electrical circuit for fitting electrochemical impedance data.

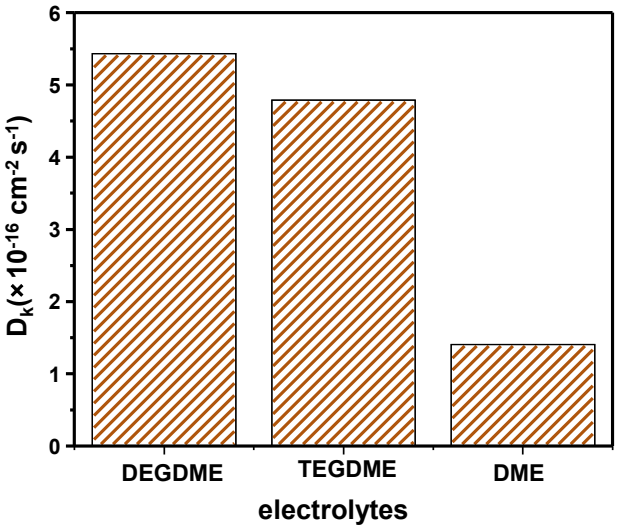

Fig. S9 Na-ion diffusion coefficients of DEGDME, TEGDME, DME.

Table 1. First charge/discharge-specific capacity and initial coulombic efficiencies of DEGDME, TEGDME, DME, and EC/DEC electrode

Samples	initial charge specific capacity (mA h/g)	initial discharge specific capacity (mA h/g)	First irreversible capacity (mA h/g)	initial coulombic efficiency (%)
DEGDME	279.0	495.4	216.4	56.3
DME	265	524.9	259.9	50.4
TEGDME	229.6	373.6	144	61.4
EC/DEC	349.3	864.3	515	40.4

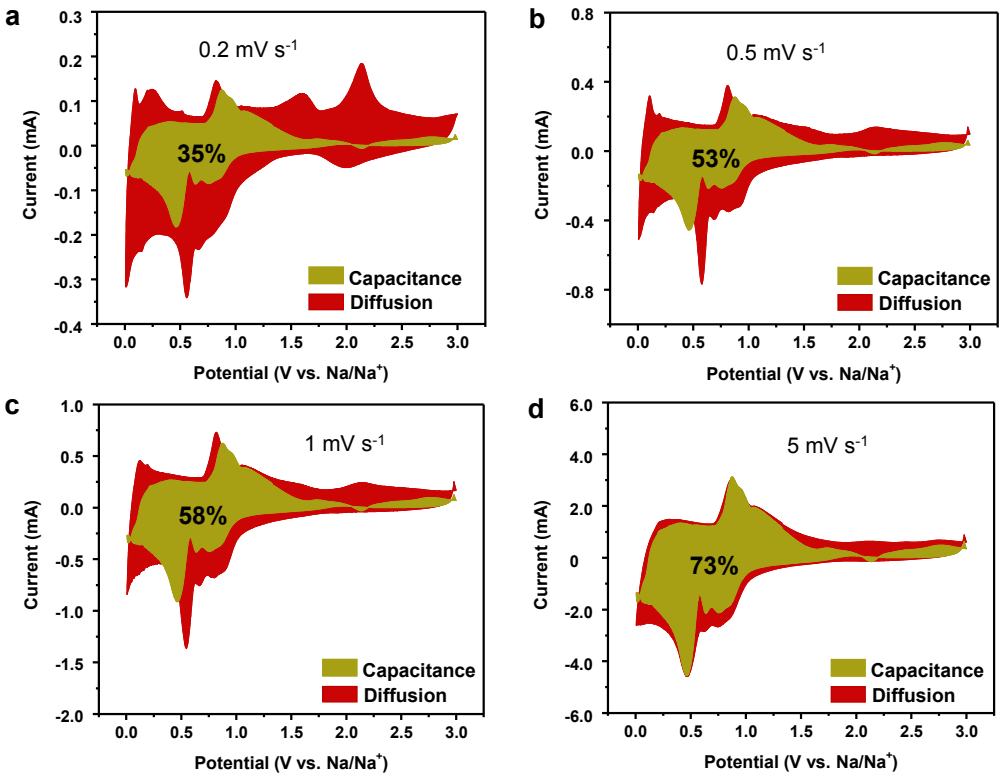

Fig. S10 Typical capacitance and diffusion contribution at (a) 0.2 mV s^{-1}, (b) 0.5 mV s^{-1}, (c) 1 mV s^{-1} and (d) 5 mV s^{-1}

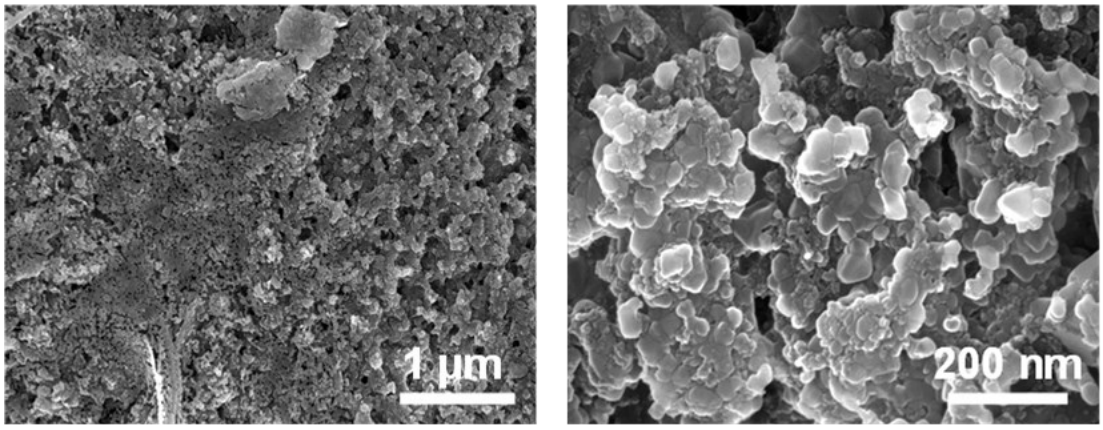

Fig. S11 SEM images of the $AlCl_3$-GIC anodes after 900 fully sodiation/desodiation cycles.

References

1. D. Su, K. Kretschmer and G. Wang, Adv. Energy Mater., 2016, **6**, 1501785.
2. H. Kim, J. Hong, G. Yoon, H. Kim, K.-Y. Park, M.-S. Park, W.-S. Yoon and K. Kang, Energy Environ. Sci., 2015, **8**, 2963-2969.
3. L. Bu, X.-X. Kuai, W.-C. Zhu, X. Huang, K. Tian, H. Lu, J. Zhao and L. Gao, Electrochimica Acta, 2020, **356**, 136804.
4. Y.-P. Shen, C. Huang, Y.-H. Li, Y. Zhou, Y.-L. Xu, Y. Zhang, Electrochimica Acta, 2021, **367,** 137526.
5. W.-J. Xu, C.-X. Lv, J. Sun and D.-J. Yang, J. Power Sources, 2019, **442**, 227184.
6. W.-W. H, D.-C. Chen, Q.-F. Li, W.-L. Liu, H.-Q. Chu and X.-H. Rui, J. Power Sources, 2019, **439**, 227072.
7. Z. Wang, L. Qie, L. Yuan, W. Zhang, X. Hu and Y. Huang, Carbon, 2013, **55**, 328–334.